Electron Phasespace Density Analysis Based on Test-Particle Simulations of Magnetospheric Compression Events

J.L. Gannon and X. Li

Laboratory for Atmospheric and Space Physics, Boulder, Colorado

The sudden appearance of a new electron radiation belt at approximately 2.5 R_e, as observed by CRRES (Combined Radiation and Release Experiment Satellite) on March 24, 1991, has been modelled by Li et al. (1993), by means of a test-particle simulation. They reproduced the observed flux levels using a guiding-center code which conserves the particles' first adiabatic invariants. The current work presented in this paper uses the output of a very similar particle tracing simulation to produce a phasespace density profile versus radial distance for the event. This work confirms the previous work and provides more detailed information about the initial particle distribution. In addition, the source population used in the Li et al. (1993) model is replaced by a flat initial phasespace density profile versus radial distance. This is done in order to test the model and to study the contribution of the initial particle distribution to the results. Under this initial distribution, with no changes to the field model, the results show that the overall flat form of the original profile is retained. As another test of the model and in order to study the contribution of the field, the model field is replaced with a symmetric (no local time dependence) electric field with full reflection, with no modifications to the source population. This leaves the phasespace density profile unchanged. We also present an argument that the third adiabatic invariant is conserved for all time during the compression, as long as the model field is azimuthally symmetric.

INTRODUCTION

On March 22, 1991, an optical flare was observed on the Sun (Blake et al., 1995). Twenty-eight hours later, at 3:41 UT on March 24, 1991 the effects of a strong shock impact were seen by the CRRES satellite (see Figure 1), which was fortuitously located at approximately 2.5 R_e, during its inbound pass on the nightside near the equatorial plane. During orbit 587, March 24, 1991, CRRES observed a very rapid ($<$ 10 seconds) four order of magnitude increase in electron flux, a unipolar magnetic field enhancement, and a bipolar electric field (see Figure 2). This is believed to be associated with an interplanetary shock from the Sun impacting the Earth's magnetosphere (Blake et al., 1995). The new highly energetic electron radiation belt produced by this event greatly affected the Earth's space environment and the intensity can be seen in

Figure 1 during the remainder of the mission (about 6 months). The new radiation belt, while decaying slowly, persisted much longer, and was observed by the SAMPEX satellite for almost ten years (Li and Temerin, 2001).

Li et al. (1993) modelled the March 24, 1991 event by representing the electric field due to magnetospheric compression and relaxation as two gaussian pulses, one incoming and one reflected, in the magnetosphere. The pertubed magnetic field was calculated from the specified electric field using Faraday's law. Figure 2a shows the integral flux data and electric and magnetic field measurements from CRRES. Figure 2b shows the results of a particle tracing code under the modelled electric field, as well as the modelled fields for comparison to the data. The sawtooth shape in both integral flux plots are particle drift-echoes, which occur as electrons drift around the Earth and return to the CRRES detector. The period of the drift echoes, about 150 seconds, approximately corresponds to the drift period of a 15 MeV electron at L=2.5, the detector position. L corresponds to the radial distance in units of Earth radii at the equator, if the Earth's magnetic field is approximately a dipole.

Li et al. (1993) were able to reproduce the drift echoes, and flux magnitudes for the first 900 seconds of the event. Other work has been done on this event, such as MHD simulations by Hudson et al. (1997) and Elkington et al. (2002). These works consolidated the idea of fast acceleration of radiation belt electrons by a travelling electric field associated with a strong interplanetary shock impact on the magnetosphere.

Because of the availability of the CRRES data, the original simulation focused on reproducing the integral flux measurements. However, a phasespace density profile versus L is subject to greater physical restraints, and because of this, would allow us further insight into the processes involved in shock induced radial transport. Phasespace density is based on the canonical coordinates of the system, from which the adiabatic invariants can be derived. Liouville's theorem states that, in the absence of sources and losses, phasespace density, f, is conserved along the trajectory of a particle, or $f = constant$ (Walt, 1996). Because of the implications of Liouville's theorem and conservation of the adiabatic invariants, phasespace density is a more physically meaningful parameter than flux or count, which are more natural for the particle detector. Because no phasespace density profile is available observationally, we must reconstruct it from the information we do have.

In order to calculate a phasespace density profile versus radial distance, we require knowledge of differential flux. CRRES satellite observations are limited to integral channels in the energy range of interest, requiring us to reconstruct the differential flux from the available models. We use a model very similar to Li et al. (1993), differing only in the exclusion of detector geometric factors and satellite motion. We retain the parameters and source population that they found to best reproduce the features of the March 24, 1991 event.

In this work, we determine the phasespace density profile versus L before and after the shock on March 24, 1991 using a particle tracing code. In addition, as a test to the code, and in order to independently study the contributions of the source population and field model to the result, we look at the effects of the Li et al. (1993) model field on an initially flat source population versus L and a field representing a symmetric, local time-independant compression on the original source population.

MODEL DESCRIPTION

The model used by Li et al. (1993) consists of an electric field model of the following form, and a magnetic field derived from it, using Faraday's law:

$$\mathbf{E}(r,t) = -\hat{e}_\phi E_0(1 - c_1\cos(\phi - \phi_0))(e^{-\xi^2} - c_2 e^{-\eta^2}) \quad (1)$$

$$\eta = [r - v_0(t - t_{ph} + t_d)]/d$$

$$\xi = [r + v_0(t - t_{ph})]/d$$

$$t_{ph} = t_i + (\frac{c_3 \mathrm{R}_e}{v0})[1 - \cos(\phi - \phi_0)]$$

where $\hat{e}_\phi$ is a unit vector in the azimuthal direction, positive eastward.

The exponential terms represent the compression and relaxation of the magnetosphere as oppositely-directed gaussian pulses. The exponents of the gaussians include a time delay. The exponential form is multiplied by a local time modulation, with the strongest point of the field corresponding with the point of impact of the impulse. The electric field looks like a wave, propagating inward and azimuthally at a constant speed, and partially reflecting at the ionosphere. The calculated magnetic field pulse is added to a simple dipole background field. The parameter $c_1 = 0.8$ affects the local time dependence, $c_2 = 0.8$ determines the amount of reflection, $c_3 = 8.0$ represents the magnitude of the propagation delay in the azimuthal direction, $t_d = \frac{2.06\mathrm{R}_e}{v_0}$ indicates the location of the reflection at $r = 1.03$ R_e, and $t_i = 81$ sec is the initial reference time. The parameters found to mimic the unipolar electric field and bipolar magnetic field observed by CRRES are $v_0 = 2000$ km/s, $E_0 = 240$ mV/m, $\phi_0 = 45\,\mathrm{deg}$ and $d = 30,000$ km. The parameters t, ϕ, and r are the time, azimuthal and radial position of the particle. Figure 3 shows several snapshots of the electric field pulse at different points in time. The pulse travels in, **E** pointing westward, and is reflected, **E**pointing eastward. The field magnitude is strongest at the point of impact, ϕ_0.

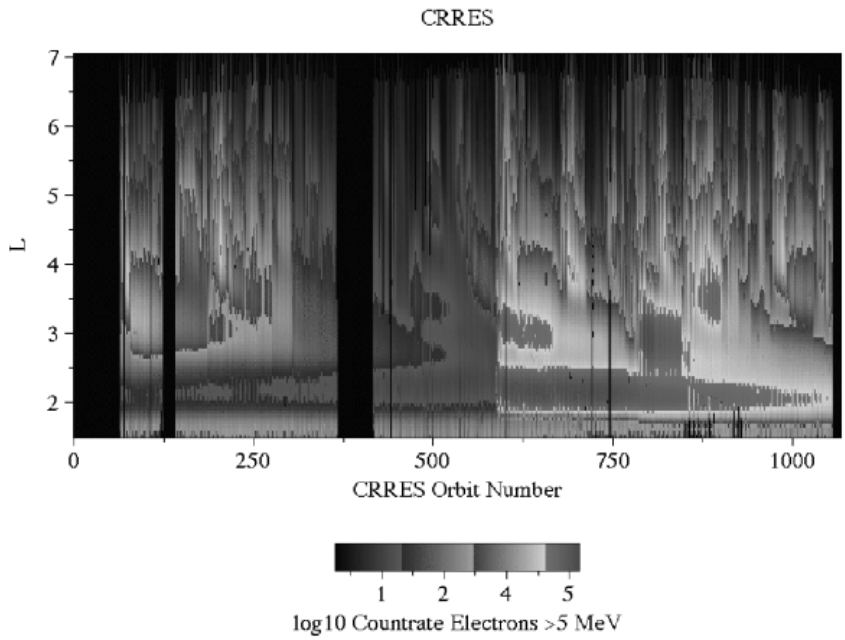

Figure 1. (Courtesy of J.B. Blake) Electron countrate measured by CRRES ($> 6\ MeV$) for the whole CRRES mission: July 1990 to October 1991. The data are binned in 0.1 L-values and the range L=1.0 to 7.0 is shown. The CRRES spacecraft was in an 18 deg-inclination geotransfer orbit (300 km x 5.2 R_e). The event of March 24, 1991 occurred at orbit 587.

Li et al. (1993) applied the field model to a test particle code following about 300,000 equatorially-mirroring electrons under the Northrop (1963) guiding center equations:

$$\dot{W} = e\dot{\mathbf{R}}_{\perp} \cdot \mathbf{E} + \frac{\mu}{\gamma}\frac{\partial B}{\partial t} \tag{2}$$

$$\dot{\mathbf{R}}_{\perp} = \frac{\hat{e_1}}{B} \times (-c\mathbf{E} + \frac{\mu c}{e\gamma}\nabla B) \tag{3}$$

In the above equations, W is particle energy, E is the electric field (modelled impulse), B is the magnetic field (calculated from the electric field pulse, plus a background dipole field), R is the radial position, $\hat{e_1}$ is a unit vector in the direction of the magnetic field, c is the speed of light, and e is the electron charge.

The initial particle distribution used by Li et al. (1993) extended from 3.0 to 9.0 R_e, every three degrees in azimuth and every 10% in initial energy from 1.0 to 9.0 MeV. A weighting was included in order to simulate a realistic electron distribution. It included a strong power law in energy (many more low energy particles than high energy particles), as well as a parabolic weighting in radial position, in order to reproduce the observation:

$$weighting = G(L) * L^2 * \sigma * W^{-7} * \frac{v}{v_d} \tag{4}$$

$$G(L) = 1 - \frac{(L - L_0)^2}{a_0}.$$

In the above, $a_0 = 7.5$ and $L_0 = 10$, and the L^2 term allowed for the fact that the area over which the source was spread increased with radial distance. The ratio of actual velocity, v, to drift velocity, v_d corrects for the fact that the guiding centers of the electrons are traced rather than the complete motion. Li et al. (1993) used σ to represent the detector response, modelling the detector geometric factors. This is not used in the current work. In addition, the original work included satellite motion. In this work, we consider the satellite to be stationary.

The limitations of the model used in this study include a constant magnetospheric shock propagation velocity, the use of a dipole background field and restriction to equatorially-mirroring particles. However, arguments can be made for using a constant velocity of propagation if the impulse, which is believed to be very sharp and fast, does not travel via fast magnetosonic modes, but instead as a propagating discontinuity (J. Lyon, private communication, 2004), which would not slow down as much in the region of interest. The use of a dipole is a reasonable simplification for the inner magnetosphere and allows us to make the arguments in the source population and model field modification sections. Tracing particles of pitch

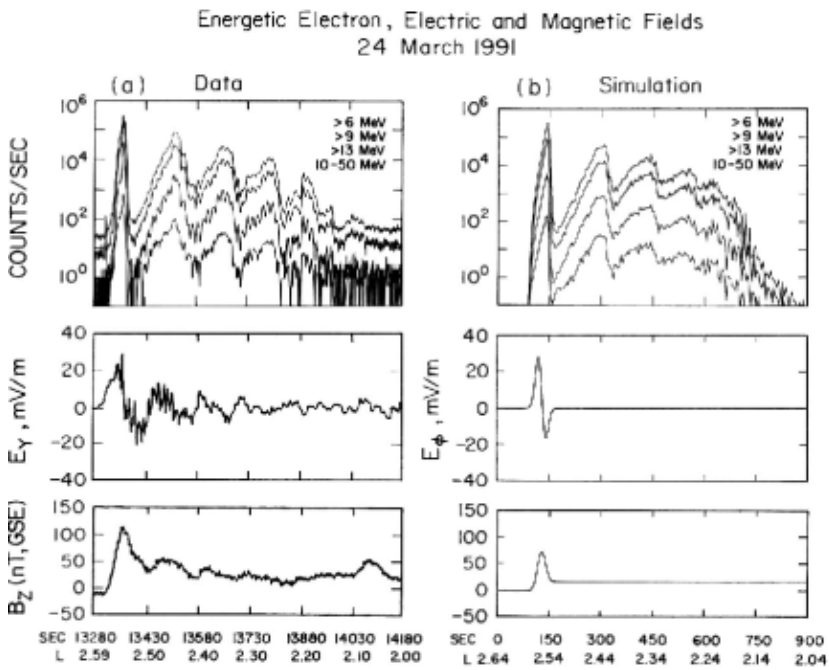

Figure 2. From Figure 1 of Li et al, GRL. Page 2403, 1993. (a) Count rate and field data taken from the CRRES satellite during the March 24, 1991 SSC. Top panel shows count rates as a function of time from four energetic electron channels measuring integral counts above 6, 9, and 13 *MeV* and also between 10-50 *MeV* [Blake et al. (1992)]. Middle and bottom panels show the measured electric field E_y in a co-rotational frame and the B_z magnetic field component with a model magnetic field subtracted, in GSE coordinates over the same time interval [Wygant et al. (1994)]. (b) Simulation results of the March 24, 1991 event by Li et al. (1993), in the same format as (a).

angles other than 90 degrees would be worthwhile, but is not computationally feasible at this point.

Figure 2b, previously mentioned, shows the simulation results of the original Li et al. (1993) work. Figure 4 shows results based on the output of the very similar simulation we used in this work. Figure 4a shows integral flux values similar to the original reproduction and data in Figure 2. Figure 4b shows a count rate versus L for particles in the simulation. This includes no detector geometric factor. It simply shows the particles seen above three energy thresholds (6, 9, 13 *MeV*) from simulation output. Figure 4c depicts the count rates versus energy of particles seen at a particular radial location, $L = 2.6$. The peak energy is about 12-13 *MeV*, which corresponds to the energy of electrons postulated to have dominated in the observed CRRES flux measurements.

PHASESPACE DENSITY CALCULATION

The original study of the event focused on reproducing the flux levels seen by the CRRES detector. In order to calculate phasespace density from simulation output, we first choose a value of the first adiabatic invariant, μ, based on the electrons' energy at $L = 2.5$, which is where we have CRRES data for comparison at the time of the March 24, 1991 event. For a relativistic electron:

$$\mu = \frac{p_\perp^2}{2m_0 B} \tag{5}$$

where $p_\perp$ is the electron's momentum perpendicular to the local magnetic field, $m_0 = 0.511\ MeV$ is the electrons rest mass, and B is the magnetic field.

From the output of the particle tracing code we select all particles within $\pm 10\%$ of the chosen μ. We then choose a time range much earlier than the shock arrival for the pre-shock analysis, and long after the shock arrival for the post-shock analysis. We want to plot phasespace density versus L, so we separate the selected particles into L-bins of 0.5, and convert the flux in each bin to phasespace density using the following relation:

$$f = \frac{j}{p^2} \tag{6}$$

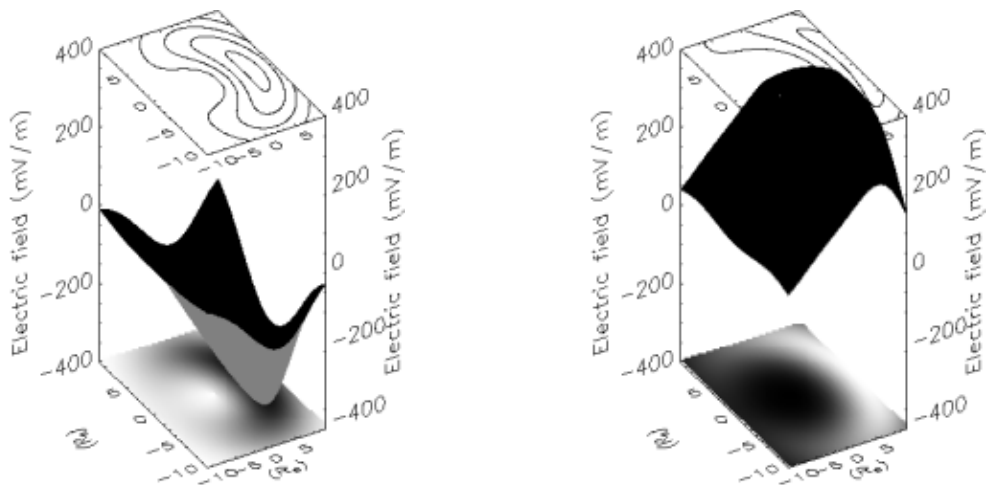

Figure 3. Snapshots at 2 times of the electric field model used by Li et al. (1993) and the current work. The Sun is to the right at a positive radial distance. Left: The incoming pulse, $E_\phi < 0$, at t=60 sec. Right: The reflected pulse, $E_\phi > 0$, at t=120 sec.

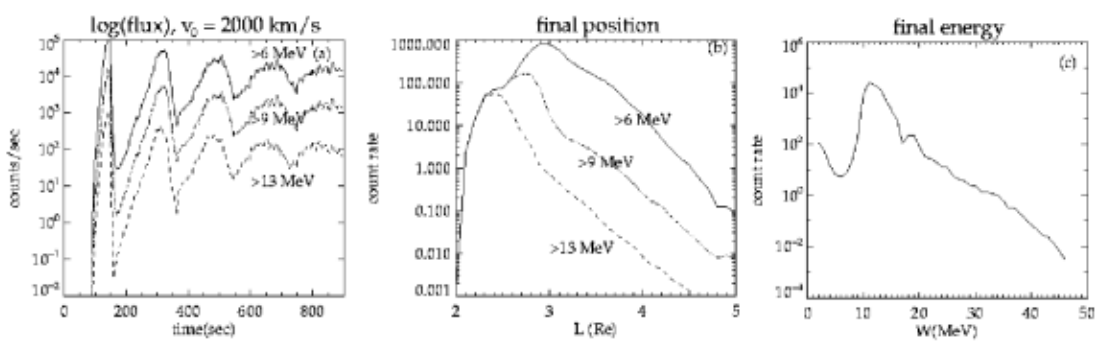

Figure 4. Simulation results for values used to simulate March 24, 1991event. a) log(count) at detector location. b) final radial position distribution of count rate for each of the four CRRES energy channels. c) final energy spectrum at detector position.

where j is differential flux and p is momentum. For equatorially mirroring particles, $p_\perp = p$. Recalling equation (5), we have:

$$f = \frac{j}{2\mu m_0 B} \tag{7}$$

We use our chosen value of μ and determine the magnetic field from the dipole relation based on the middle of each L-bin.

In order to make the phasespace density levels realistic, we scale them to match the flux data available from CRRES. The equation for phasespace density, (6), requires differential flux, for which we do not have data available for direct comparison. However, the simulation results of Li et al. (1993), incorporated with detector geometric factors, have been matched to the observed integral countrate, and thus we can use the model output to estimate what differential flux measurements CRRES would have seen. For example, we select an energy

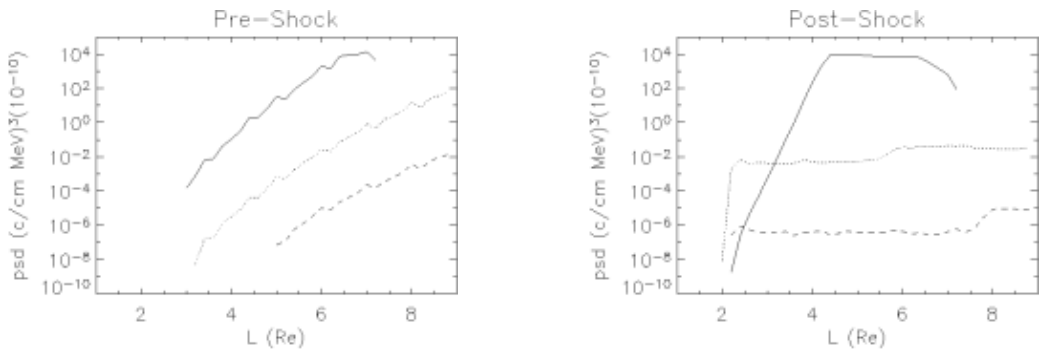

Figure 5. Left: Pre-shock phasespace density profile derived from the source population used by Li et al. (1993) to model the March 24, 1991 event. Right: Post-shock phasespace density profile from the output of the Li et al. model of the March 24, 1991 event. solid: $\mu = 2077\ MeV/G$, dotted: $\mu = 11852\ MeV/G$, dashed: $\mu = 45898\ MeV/G$

range of 14-16 MeV and, for a chosen simulated channel ($>$ 13 MeV) we count the number of particles in the 14-16 MeV range that are seen from 300 - 600 seconds (in the simulation, the field interacts with the particles from $t = 80 - 150\ s$), applying the weighting used by Li et al. (1993) to obtain the countrate that a detector would have recorded:

$$countrate = \sum \sigma \times weight(L_0, W_0)$$

where σ represents the geometric factor and $weight(L_0, W_0)$ represents all additional weighting based on initial position and energy. This gives us a value for differential flux including detector response. Then, we divide the countrate by the average response that the channel of the detector would have to electrons of 14-16 MeV, to give the differential flux:

$$j_{real} = \frac{countrate}{\sigma_{effective}}$$

where $\sigma_{effective}$ is the average detector response. Using the specified μ for each phasespace density curve we wish to scale, the dipole value of the magnetic field at a particular radial distance, and the calibrated differential flux from the above method, we use equation (7) to calculate what the phasespace density should be at that radial distance. This process was done for phasespace densities with other μ as well.

Phasespace Density Analysis of March 24, 1991

Figure 5 shows the calculated phasespace density profile of the particle population, pre-shock and post-shock, versus L-value. The three lines on each plot represent different values of the first adiabatic invariant. The middle line represents 11852 MeV/G, corresponding to about 15 MeV at 2.5 R_e, which is the energy of the bulk of the particles at that position, post-shock, as seen by CRRES and simulation results (see Figure 4c). In the pre-shock phasespace density plot (Figure 5a), there are no particles at $L = 2.5$. Post-shock, particularly in the μ range corresponding to about 15 MeV at 2.5 R_e, there are particles extending Earthwards to almost 2.0 R_e. There is a peak in flux versus L at approximately $L = 2.5 - 2.6$ (Figure 1) after the impulse. This peak in flux was also reproduced by simulation (Figure 4b, $> 13\ MeV$ range), which shows them varying somewhat with L for different modelled integral channels.

The sudden energization process that produced the effects seen by CRRES is a drift-resonant process, where the resonance is determined by an electron's first invariant for a given model field. Under the model, particles of the same energy and radial position, but different local time, see different field strengths, such that particles in the right location at the right time are energized more than others, or, in other words, are resonant with the pulse. The particles of 11852 MeV/G are nearest those in the peak of the final energy spectrum (see Figure 4c), and can be considered most resonant. We see no true peaks in phasespace density, as shown in Figure 5b. Local heating (by which we mean a process that violates a particle's first adiabatic invariant) could produce a peak, as the more abundant lower energy particles are energized at a particular radial distance. However, this radial transport process, which is μ-conserving, produces no peaks in phasespace density. If a particle were to remain at a particular L and be energized, conservation of the first adiabatic invariant would be violated. Even if there is an initial existing peak, the natural tendency of such a process would be to reduce the peak. The drop-offs at the ends of each curve occur due to pre-existing phasespace density holes as a result of the initial distribution. Li et al. (1993) speculated that there was insufficient phasespace density available at $L < 6$ to produce the four order of magnitude increase seen at $L = 2.5$ by the CRRES detector while conserving the first adiabatic invariant, μ. Li et al. (1993) determined

that electrons would have to have come from $L > 6$. In the Li et al. (1993) simulation, the bulk of the particles were accelerated from the farthest L-shells in the source population, i.e. $L = 7-9$. These results are reflected in the phasespace density profile versus L.

Comparison With Polar Quiescent Radiation Belt Data

In order to understand if our simulation results are of a reasonable magnitude, we compare with available known phasespace density measurements. Selesnick et al. (1997) show data from the Polar satellite during a quiescent period, which they describe as a steady state of particle diffusion in the magnetosphere. They look at phasespace density profiles versus L for about 100 days of 1996. We can use these data as a baseline to see if our derived phasespace densities are realistic. We cannot make a direct comparison, as their selected values of the first adiabatic invariant are lower than the values of interest in our case. However, we can show limited comparison to several features. In our profile, post-shock, between L = 3.0 and L = 5.5, we see a several order of magnitude increase in phasespace density, especially in the higher values of the first adiabatic invariant. Polar data show the same trend, especially early in the time period they observed, following a particle injection, for a first adiabatic invariant of 6000 MeV/G. Comparing actual phasespace density absolute magnitudes is more difficult, as phasespace density varies significantly with time and we are looking at only one instance in time. In the Polar data, for a μ of 6000 MeV/G, the maximum phasespace density reached was approximately 100 $(10^{-10})(cmMeV/c)^{-3}$. Under our simulation for a μ of 11852 MeV/G, a higher value of μ, we expect a lower phasespace density. The maximum phasespace density reached in our simulation was about 10 $(10^{-10})(cmMeV/c)^{-3}$, which is not inconsistent because of the different values of μ.

Initial Distribution Modifications - Flat Profile Versus L

As a test to the model, and in order to study the contribution of the source population, we consider the effect of the same model field on an initially flat phasespace density profile. Because of the continually evolving nature of phasespace density, a flat profile is not typically seen in nature, but it is not unphysical, especially on small scales. In this case, the initial electron distribution was forced to be flat in phasespace density versus L by adjusting the weighting. This was achieved by modifying the dependence on radial position and the energy weighting. The parabolic form based on position, G(L) in equation (4), was replaced with a power law, L^{-2}. The weighting in energy was removed by adding an additional factor W^1 in order to negate the weighting implicitly included in the 10% increase in initial energy distribution from 1.0 to 9.0 MeV. This could also be achieved by adjusting the energy spectrum from W^{-7} to $W^{1.5}$, without changing $G(L)$. Although the same results are achieved, a positive power law, in general, is unrealistic, as it implies particle numbers increasing with energy.

Figure 6 shows the post-shock curves never peak above the pre-shock curves. They remain flat except near the boundaries where there are existing phasespace density holes. Particles spread out in L, and because the total number of particles is approximately conserved (less those few lost past the outer bounds of the simulation), an increase in phasespace density at one radial distance necessitates a decrease at another. This is an illustration of the idea that a μ-conserving process can not lead to increases in phasespace density versus L above the initially assumed flat phasespace density distribution. A particle cannot remain at the same radial distance and increase its energy without changing its μ.

Field Model Modifications – Azimuthally-Symmetric Compression

What happens in an azimuthally-symmetric compression case? In the Li et al. (1993) simulation, an 80% reflection was used to match field measurements from CRRES on the simulation time scale, and a local-time dependence of the strength of the field was included. In addition to removing the local-time dependence of the compression, we use a 100% reflection (complete relaxation to the initial field configuration) for this part of the study. Figure 7 shows that pre- and post-shock phasespace densities are identical, apart from statistics. In the previous cases, even if there were 100% reflection, some of the particles would remain energized even after the system has relaxed to the initial dipole configuration, a long time after the compression has passed, implying a breaking of the third adiabatic invariant. In the symmetric case, the particles return to the initial distribution – no net energization.

Is the third adiabatic invariant conserved for the symmetric case? The definition of the third adiabatic invariant is:

$$\phi_M = \int B \cdot dA \tag{8}$$

where ϕ_M is magnetic flux through a surface A. This can be thought of as the number of magnetic field lines contained within the particle's drift path, such that the surface A is the area enclosed by that drift path. Because the field we are using is a static dipole before and after the shock, a particle that returns to its original radial distance returns to its original ϕ_M. Therefore the third adiabatic invariant is the same for the pre- and post-shock instances.

Can we say the same for every point in time in between? First, consider the motion of a cold electron during a compression. Because the electron must follow field lines, which cannot cross, the magnetic flux inside the drift path will not

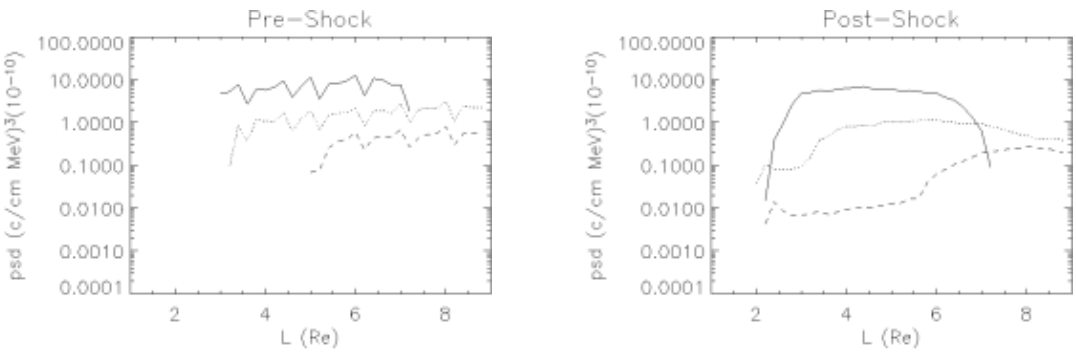

Figure 6. Left: Pre-shock phasespace density profile from the output of the Li et al. model using modified source population. Right: Post-shock phasespace density profile from the output of the Li et al. model using modified source population. solid: $\mu = 2077\ MeV/G$, dotted: $\mu = 11852\ MeV/G$, dashed: $\mu = 45898\ MeV/G$

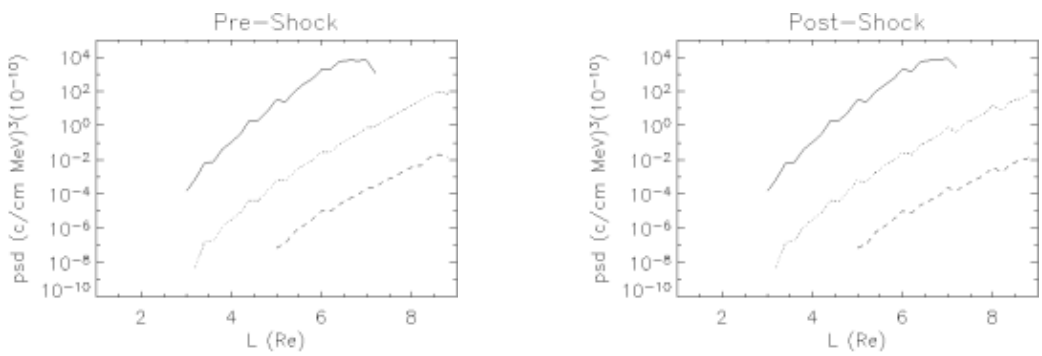

Figure7. a) Pre-shock phasespace density profile from the output of the model using symmetric compression parameters. b) Post-shock phasespace density profile from output of the model using symmetric compression parameters. solid: $\mu = 2077\ MeV/G$, dotted: $\mu = 11852\ MeV/G$, dashed: $\mu = 45898\ MeV/G$

change as the electron moves inward (see Figure 8). The situation is no different than the beginning or end of the compression – the number of field lines in the drift path is unchanged and ϕ_M remains constant. Because the only mechanism for radial displacement under this model is $E \times B$-drift, which is energy independent, this argument can be generalized to include energetic particles, i.e., ϕ_M still remains constant. For azimuthally symmetric magnetic fields, when the guiding center approximation is valid, the third adiabatic invariant is conserved at all points along the particles' drift path. We have made no assumptions about the relative time scales of the pulse and particle drift in this argument. In our case, the time scale of the pertubation is not significantly longer than the particles' drift. A pertubation time scale longer than the drift means the corresponding invariant is conserved, but a pertubation time scale shorter than the drift does not necessarily mean the invariant is not conserved. In this azimuthally-symmetric compression example, the third adiabatic invariant is conserved, regardless of the time scale of the pertubation. Figure 9 shows the drift path, radial position and energy of a single particle. It shows that the individual particle does return to its original radial position.

In the asymmetric compression case, ϕ_M is not conserved due to the local time dependence, in which the particles see a different strength electric field at different locations. In other words, the more resonant particles see more of the field for a longer amount of time. In the symmetric case, the particles see the same field independent of their velocity or position.

SUMMARY

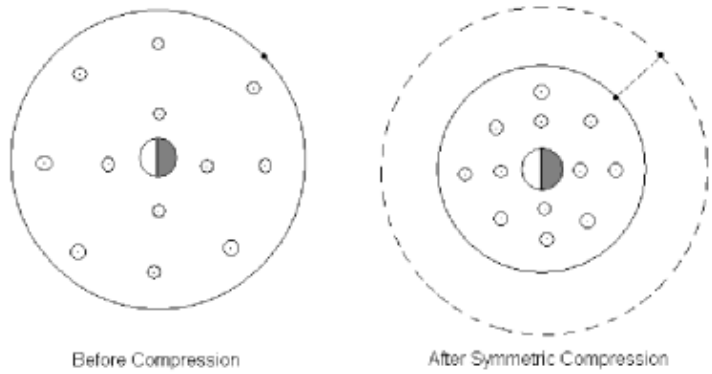

Figure 8. (Courtesy of E. Burin des Roziers) Diagram of a cold electron following a field line during a symmetric compression. Left: The solid circle indicates the initial radial position in a dipole field. Right: After the field is compressed, the electron is now at the new position (solid line). The dotted line is the original position in the left panel. Because magnetic field lines cannot cross, the flux enclosed in both solid circles is the same.

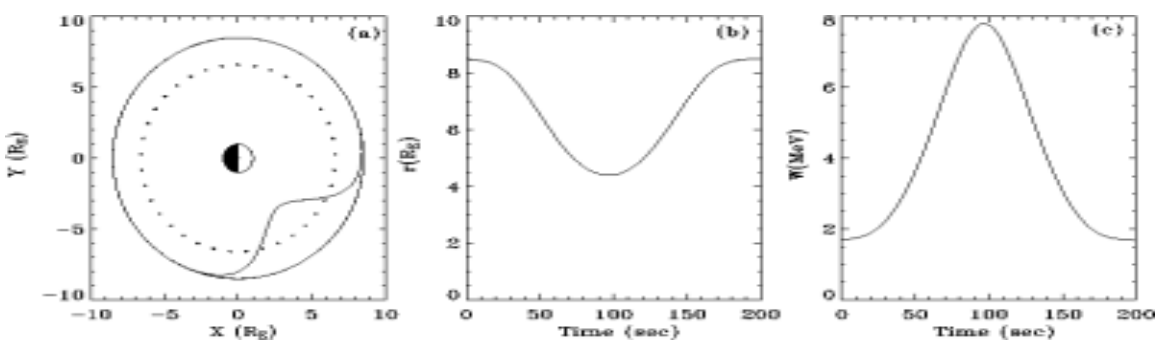

Figure 9. Single particle example under the symmetric field model. The electron begins with an energy of 1.7 MeV, a radial position of 8.5 R_e and an azimuthal position of 4 deg (near noon). Panel a) shows drift path, b) shows change in radial position, and c) shows the electrons energy versus time. Panel (b) and (c) only cover the interaction with the compression. (t=0 is not simulation onset time)

A phasespace density profile versus L of the March 24, 1991 event was produced using output of the particle-tracing simulation by Li et al. (1993), confirming earlier observations by CRRES which showed there was insufficient phasespace density at $L < 6$. Additional studies were done using the same electric field model, but assuming an initially flat phasespace density versus radial distance profile. This was done to study the contribution of the initial particle distribution to the results, as well as a test of the model. The phasespace density profile remains flat except near the boundaries, and the post-shock curves never surpass the pre-shock curves, illustrating that such a μ-conserving radial transport process cannot produce increases in phasespace density above an initially assumed flat phasespace density profile of a given μ versus L. As another test of the model and in order to study the contribution of the field, a symmetric (no local time dependence) electric field with full reflection is used, with no modifications to the Li et al. (1993) source population. This yields a phasespace density profile identical to the initial phasespace density profile. Under an azimuthally-symmetric compression, particles conserve the third adiabatic invariant at all times during the compression, in addition to the first adiabatic invariant, as long as the guiding center approximation is valid. These tests, together with the phasespace density analysis, illustrate

the significance of both the initial particle distribution and the actual fields associated with such compression events.

Acknowledgements

We are thankful for both reviewers for their helpful comments and suggestions. This work was supported by NASA grants (NAG5-10474 and -13518) and NSF grants (ATM-0233302 and -0101351)

References

Blake J.B., W.A. Kolasinski, R.W.Rillius, and E.G. Mullen, Injection of electrons and protons with energies of tens of MeV into L¡ 3 on March 24, 1991, *Geophys. Res. Lett.*, *19*, 821, 1992.

Elkington, S.R., M.K. Hudson, M.J. Wiltberger, J.G.Lyon, MHD/particle simulations of radiation belt dynamics, *Journal of Atmospheric and Solar-Terrestrial Physics*, 64, 607-615, 2002.

Hudson, M.K., A.D. Kotelnikov, X. Li, I. Roth, M. Temerin, J. Wygant, J.B. Blake, M.S. Gussenhoven, Simulation of proton radiation belt formation during the March 24, 1991 SSC, *Geophys. Res. Lett.*, *22*(3), 291, 1995.

Hudson, M.K., S.R. Elkington, J.G. Lyon, V.A. Marchenko, I. Roth, M. Temerin, J.B. Blake, M.S. Gussenhoven, J.R. Wygant, Simulations of radiation belt formation during storm sudden commencements, *J. Geophys. Res.*, vol. 102, A7, 14087-14102, 1997.

Li, X., I. Roth, M. Temerin, J. Wygant, M. K. Hudson, and J. B. Blake, Simulation of the prompt energization and transport of radiation particles during the March 24, 1991 SSC, *Geophys. Res. Lett.*, *20*, 2423, 1993.

Li, X., M.K. Hudson, J.B.Blake, I. Roth, M. Temerin, and J.R. Wygant, Observation and simulation of the rapid formation of a new electron radiation belt during March, 24, 1991 SSC, *Workshop on the Earth's Trapped Particle Environment, AIP Conference Proceedings*, 383, 109, AIP Press, Woodbury, NY, 1996.

Li, X. and M. Temerin, The Electron Radiation Belt, *Space Science Reviews*, 95, 569-580, Kluwer Academic Publishers, 2001.

Northrop, T.G., *The Adiabatic Motion of Charged Particles*, Interscience Publishers, New York, 1963.

Schulz, M., The magnetosphere, in *Geomagnetism*, vol. 4, edited by J.A. Jacobs, p. 87, Academic, San Diego, California, 1991.

Selesnick, R.B, J.B. Blake, W.A. Kolasinski and T.A. Fritz, A quiescent state of 3 to 8 MeV radiation belt electrons, *Geophys. Res. Lett.*, *24*(11), 1343-1346, 1997.

Temerin, M., I. Roth, M. K. Hudson, J. R. Wygant, New paradigm for the transport and energization of radiation belt particles, *AGU, Eos*, Nov. 1, 1994, page 538.

Walt, M., Source and Loss Processes for Radiation Belt Particles, Geophysical Monograph - Radiation Belts Models and Standards, J.F. Lemaire, D. Heyderickx, D.N. Baker, eds., 1996.

Waters, C.L., B.G. Harrold, F.W. Merik, J.C. Samson, and B.J. Fraser, Field line resonances and waveguide modes at low latitudes, *J. Geophys. Res.*, 21, A4, 7763-7774, 2000.

Wygant, J., F. Mozer, M. Temerin, J. Blake, N. Maynard, H. Singer, M. Smiddy, Large amplitude electric and magnetic field signatures in the inner magnetospher during injection of 15 MeV electron drift echoes, *Geophys. Res. Lett.*, *21*(16), 1739-1742, 1994.

Jennifer Gannon
LASP, 1234 Innovation Dr.
Boulder, CO 80303
gannonjl@colorado.edu

Xinlin Li
LASP, 1234 Innovation Dr.
Boulder, CO 80303
Xinlin.Li@lasp.colorado.edu